Fast phase recovering from a single closed fringe pattern

Oscar S. Dalmau-Cedeño[1], Mariano Rivera[1] and Ricardo Legarda-Saenz[2]
[1]Centro de Investigacion en Matematicas A.C.
Apdo Postal 402, Guanajuato, Gto. 36000 Mexico
[2]Facultad de Matematicas, UADY
Mérida, Yuc. Mexico
{dalmau,mrivera}@cimat.mx, rlegarda@tunku.uady.mx

A new framework for phase recovering from a single fringe pattern with closed fringes is proposed. Our algorithm constructs an unwrapped phase from previously computed phases with a simple open fringes analysis algorithm; twice applied for analyzing horizontal and vertical oriented fringes, respectively. That reduces the closed fringe analysis problem to chose the better phase between the two oriented computed phase and then to estimate the local sign. By propagating the phase sign (and a DC term) by regions (named here *tiles*), instead of a pixelwise phase propagation, we become more robust and faster the analysis of closed fringe patterns. Additionally, we proposed a multigrid refinement for improving the final computed phase.

OCIS codes: 120.2650, 100.3190, 120.3180, 120.5050, Closed Fringe Analysis

1. Introduction

Recent complex experimental setups have made possible to acquire simultaneous interferograms with known phase steps that can be analyzed with simple algorithms. However, hostile industrial environments and the complexity of the needed experimental setups make necessary to continue the development and the improvement of algorithms for computing the phase from a single closed fringe pattern (FP). In this work we present a robust to noise and computationally efficient algorithm for phase recovery from a single closed FP. Computing the phase in this situation is still a challenging problem that has attracted the attention of researchers for analyzing transient events as, for instance, mechanical vibrations and deformations. Thus the development of close FP analysis algorithms has become a prolific research subject. One can observe two approaches to the problem, one based on a regularized propagation of the phase (or the sign) which seminar work is Ref. [1] and other based on operators and analytical transforms theory [2–4]. A popular closed FP analysis method is the named Regularized Phase Tracker (RPT), it was initially proposed by Servin *et al.* in Ref. [5] and then improved in Ref. [6]. Posteriorly, Legarda and Rivera [7] accelerated the Regularized Phase Tracker convergence by using the linearization strategy reported in Ref. [8] and introduced the fringe modulation (contrast) factor. Also in [8], Rivera proposed a phase propagation algorithm that has shown to be robust to noise, see experiments in Ref. [9]. Recently Estrada et al. [10] proposed a pixelwise local phase computation by using locally adaptable quadrature filters [11]. In this case, the nonlinear optimization is achieved by taking as initial condition the previously computed pixel phase and the neighborhood (window) that surrounds the pixel of interest. A similar approach was presented by Kemao and Soon [12]. However, differently to our work, in [12] the vertical and horizontal local frequencies are computed by using an exhaustive search in a RPT–based cost function and the sign is then determined by imposing local smoothness. The disadvantage of last procedures is the computational time required in the pixelwise processing.

Differently to above listed propagation based works, we select a phase between two vertically and horizontally oriented quadrature filter responses, in particular we used the simple ones proposed by [13] and [14], although our framework admits to use more sophisticated (and robust to noise) quadrature filters. In this work we propose a *tile*–based approach for computing the phase sign at each *tile* and a procedure for assembling a smooth global phase. Such a *tile*–based approach has been previously used for phase unwrapping [15], but not, in the best of our knowledge, for recovering the local sign in closed fringe analysis. Another problem that has not been addressed is the automatic sign estimation. Then, the main problem with closed fringes is how to assemble all the *tiles* for computing a globally consistent result. Our proposal can be seen as a novel framework for analyzing closed fringe patterns, and consists of the following steps:

1. Define a rectangular tessellation (each component is here named *tile*) in the domain of interest. (Subsection 2.A)
2. Compute a fringe orientation measure. (Subsection 2.A)
3. For each *tile*, compute the response of the best oriented quadrature filter and unwrap the *tile*-phase. (Subsection 2.B)
4. Construct a coarse phase by starting at a seed *tile* and propagating the phase by computing the adjacent *tile*-phase sign and DC. (Section 3)
5. Refine (filter) the coarse phase to obtain a final smooth phase. (Section 4)

In this work, we use simple rectangular tessellations for decomposing the domain of interest. Quadrature filters (step 3) are implemented with wide-band quadrature filters and fringe orientation is computed based on the structure tensor [16]. This paper is organized following the above presented framework. In section 2 we present our notation and propose a fringe orientation measure, based on the Knutsson structure tensor [16]. Also we review the phase estimation with two wide-band quadrature filters orthogonally oriented for analyzing horizontal and vertical fringes, respectively. An advantage of such filters is that they can be efficiently computed in the frequency domain using one direct and two inverse fast Fourier transforms. Such wide-band quadrature filters were used by Kreis [14]. Afterwards, Judge *et al.* used the horizontal and vertical wideband quadrature filter for unwrapping noisy and inconsistent wrapped phase maps [15]. The implementation of the step 4 of our framework is presented in section 3. Such procedure is the main contribution of this work. we propose a phase growing mechanism that uses the oriented quadrature filter responses and the local fringe properties. The phase propagation is efficiently performed by a successive growing of a seed phase. Such a phase growing process is achieved in relatively large spatial regions, named here *tiles*. In the low-noise case, the grown *tile*–based phase can be considered the final estimation. On the other hand, for the high-noise case, the phase in the *tile* region may be corrupted and need to be filtered. The phase refinement step (step 5) is presented in section 4. Our multigrid refinement procedure is a variant of the algorithm proposed in Ref. [8] (and extended to phase stepping in Ref [17]). Such a multigrid strategy accelerates considerably the convergence ratio of the refinement process. The method performance is demonstrated by experiments in section 5. Finally our conclusions are given in section 6.

2. Tesellation, Fringe Orientation and Local Phase

In this section we explain the steps 1, 2 and 3. These steps are based on standard and well known algorithms for computing local orientation in image analysis and local phase in fringe analysis. We remark that, in this point, we use a simple approach for demonstrating the framework performance, but our framework accepts more complex and robust procedures for computing the local orientation and phase. However, such an investigation is out of the scope of this work.

2.A. *Fringe Orientation Measure*

The image model for an FP is given by:

$$I(r) = a(r) + b(r)\cos[f(r)] + \eta(r), \quad r \in \mathcal{L}; \tag{1}$$

where $r = [x, y]^T$ denotes a pixel position in the regular lattice $\mathcal{L}$, a and b are the illumination components (background and contrast, respectively), f is the phase to estimate and η is independent additive noise.

We define a *tile* as an ordered triad: a window, an orientation vector and an orientation quality measure. We denote the *tile* by $\mathcal{P} = (\mathcal{W}^{\mathcal{P}}, \mathcal{O}^{\mathcal{P}}, \mathcal{B}^{\mathcal{P}})$ where $\mathcal{W} \subset \mathcal{L}$ is a rectangular region (window), $\mathcal{O}^{\mathcal{P}}$ is a vector that indicates the fringe *local orientation* and $\mathcal{B}^{\mathcal{P}}$ is an *orientation confidence measure*. We assume a non–overlapped and complete tessellation:

$$\mathcal{W}^{\mathcal{P}} \cap \mathcal{W}^{\mathcal{Q}} = \emptyset, \forall \mathcal{P} \neq \mathcal{Q}$$

and

$$\bigcup_{\mathcal{P}} \mathcal{W}^{\mathcal{P}} = \mathcal{L}.$$

Although others techniques can be used for computing local orientation [4, 18], in this work we based our measure on the Knutsson's structure tensor, $\mathbf{T}$, of each *tile* [16, 19–22] :

$$\mathbf{T}^{\mathcal{P}} \;=\; \frac{1}{\sharp\mathcal{P}} \begin{pmatrix} \sum_{r\in\mathcal{P}} I_x^2 & \sum_{r\in\mathcal{P}} I_x I_y \\ \sum_{r\in\mathcal{P}} I_x I_y & \sum_{r\in\mathcal{P}} I_y^2 \end{pmatrix}; \tag{2}$$

where $r \in \mathcal{P} \iff r \in \mathcal{W}^{\mathcal{P}}$, $\sharp\mathcal{P}$ denotes the number of pixels in the region $\mathcal{W}^{\mathcal{P}}$ and $I_t \overset{def}{=} \partial I/\partial t$ for $t \in \{x, y\}$ denote the partial derivatives. The *tile* orientation is determined by the eigenvector associated with the largest tensor eigenvalue, *i.e.* of $\mathbf{T}^{\mathcal{P}}$:

$$\mathcal{O}^{\mathcal{P}} \;=\; \begin{bmatrix} \mathbf{T}_{11}^{\mathcal{P}} - \mathbf{T}_{22}^{\mathcal{P}} \\ 2\mathbf{T}_{12}^{\mathcal{P}} \end{bmatrix}. \tag{3}$$

Such an orientation corresponds to the mean orientation of the level sets in the fringe pattern at the region defined by the *tile*. In the case of noisy phases, although the orientation is computable, this is not well defined at local minima, local maxima or saddle points. Therefore we need a measure of how well oriented the local fringe patterns are. Thus, let $\lambda_1^{\mathcal{P}} \geq \lambda_2^{\mathcal{P}}$ be the eigenvalues of $\mathbf{T}^{\mathcal{P}}$, then a large rate between $\lambda_1^{\mathcal{P}}$ and $\lambda_2^{\mathcal{P}}$ indicates a preferred orientation of the fringes along the first eigenvector $\mathcal{O}^{\mathcal{P}}$ and $\lambda_1^{\mathcal{P}}$ indicates the significance of such an orientation. Therefore a local orientation measure of the FP is the *tensor's coherence* [21]: $\mathcal{C}^{\mathcal{P}} = \left[(\lambda_1^{\mathcal{P}} - \lambda_2^{\mathcal{P}})/(\lambda_1^{\mathcal{P}} + \lambda_2^{\mathcal{P}})\right]^2$; that is equivalent to

$$\mathcal{C}^{\mathcal{P}} \;=\; \frac{(\mathbf{T}_{11}^{\mathcal{P}} - \mathbf{T}_{22}^{\mathcal{P}})^2 + 4(\mathbf{T}_{12}^{\mathcal{P}})^2}{(\mathbf{T}_{11}^{\mathcal{P}} + \mathbf{T}_{22}^{\mathcal{P}})^2}. \tag{4}$$

Now we propose a local quality measure (an *orientation confidence measure*) by taking into account the orientation and the significance of the fringes:

$$\mathcal{B}^{\mathcal{P}} \;=\; \lambda_1^{\mathcal{P}} \mathcal{C}^{\mathcal{P}}. \tag{5}$$

Therefore $\mathcal{B} \in \mathbb{R}^1$ states an order relationship of the form $\geq$ between the *tiles* in the set of all *tiles* $\mathfrak{P}$. Then we say that $\mathcal{P}_1$ is better oriented than $\mathcal{P}_2$ iff its orientation quality measure $\mathcal{B}^{\mathcal{P}_1}$ is greater than $\mathcal{B}^{\mathcal{P}_2}$; i.e. $\mathcal{P}_1 \geq \mathcal{P}_2 \iff \mathcal{B}^{\mathcal{P}_1} \geq \mathcal{B}^{\mathcal{P}_2}$; similarly $\mathcal{P}_1 < \mathcal{P}_2 \iff \mathcal{B}^{\mathcal{P}_1} < \mathcal{B}^{\mathcal{P}_2}$. To illustrate the above concepts, we show in Fig. 1(a) a graphic representation of the tensors associated to each *tile*; *i.e.* the level set of the quadratic form: $r^T[(\lambda_1 + \lambda_2)\mathbf{I} - \mathbf{T}]r = c$ (inertia tensor); for a fixed constant c, where $\mathbf{I}$ denotes the identity matrix. In Figs. 1(b) and 1(c) we show the *tensor coherence map*, $\mathcal{C}$, and the quality map, $\mathcal{B}$, respectively.

2.B. Oriented Quadrature Filters

Let $\tilde{I}(u, v) = \mathcal{F}\{I(x, y)\}$ be the Fourier transformation of the fringe pattern I, where (u, v) are the coordinates in the frequency domain. Then, we denote by ϕ_u the wrapped phase computed by applying a quadrature filter to $\tilde{I}$ that allows to pass only positive u–frequencies. Similarly, the wrapped phase ϕ_v results from applying a quadrature filter that allows to pass positive v–frequencies. In this work, for illustration purposes, we use the simple but computational efficient quadrature filters reported by Macy [13] and Kreis [14]. We remark that the computed local phase can be improved if more robust to noise quadrature filter banks were used, for instance Gabor's Filters [23], Monogenic Filters [9, 24] or Riesz's transform [2–4]. Fig. 2 shows the ϕ_u and ϕ_v phases for two fringe patterns: with open and closed fringes. One can see the well-known sign ambiguity in the corresponding phase of the closed fringe pattern. In this work, we present a computationally efficient method for estimating the true phase, f, from the wrapped phases $[\phi_u, \phi_v]$ by using the local fringe orientation.

The unwrapped phase $\tilde{\phi}^{\mathcal{P}}$ is computed at each *tile* $\mathcal{P}$. Given that it is very probable to have open fringe patterns in the relatively small regions defined by the *tiles*, then the *tile*-phase may be computed with standard fringe analysis methods [13, 14, 25, 26]. Depending on the local orientation of the fringes, the unwrapped phase at each *tile* are obtained from ϕ_u or ϕ_v. Therefore, ϕ_u is preferred over ϕ_v if the fringes are vertically oriented, as in first column of Fig. 2. Conversely, ϕ_v is preferred over ϕ_u if the fringes are horizontally oriented. Fig. 3(a) shows in black the preferably vertical-oriented *tiles*, and in white the horizontal-oriented *tiles*. The *tile*-based phase computation process is defined by:

$$\tilde{\phi}^{\mathcal{P}} = \begin{cases} W^{-1}(\phi_u^{\mathcal{P}}) & \text{if } |\mathbf{T}_{11}^{\mathcal{P}}| \geq |\mathbf{T}_{22}^{\mathcal{P}}|, \\ W^{-1}(\phi_v^{\mathcal{P}}) & \text{otherwise;} \end{cases} \tag{6}$$

where W^{-1} denotes the unwrapping phase operator. In this work we implement W^{-1} by using the half-quadratic convex unwrapping algorithm presented in Ref. [27]. The unwrapping algorithm converges in few iterations because the *tile* area is relatively small and the wrapping order (number of fringes in the *tile*) is, in general, small too. Fig. 3(b) shows the unwrapped phase mosaic $\tilde{\phi}$ corresponding to the shown FP in the first column in Fig. 2. Except for the *tile*-sign and the constant *tile*-DC, the phase is correctly estimated in a large region of the PF. The problematic *tiles* are those with an undefined fringe orientation, *i.e.* those with a small $\mathcal{B}$ value. For instance, the *tiles* allocated at the fringe centers. Then we propose to choose a seed *tile* (the one with the largest $\mathcal{B}$ value) that could easily be unwrapped. Afterwards we grow the solution by including the phase *tile* with better local orientation. This process is iterated up to all the *tiles* are included. In these way we leave for the last poorly oriented *tiles* (those with small $\mathcal{B}$ values). The details of the propagation procedure are presented in next section.

3. Tile-based phase propagation

3.A. Mathematical description

We define the phase propagation sequence, U, by using the quality map. The propagation sequence is a *tiles* ordered list $U = [\mathcal{P}_1, \mathcal{P}_2, \ldots, \mathcal{P}_N]$ such that the i^{th} *tile* is the one with the largest quality measure in the neighborhood $\mathcal{N}_{U_i}$ of the sublist $U_i = [\mathcal{P}_1, \mathcal{P}_2, \ldots, \mathcal{P}_{i-1}]$; where the neighborhood is defined as

$$\mathcal{N}_U = \{\mathcal{Q} \in \mathfrak{P} \backslash U : \exists (r,s), s \in \mathcal{Q}, r \in \mathcal{P}, \mathcal{P} \in U, |r-s| = 1\}, \tag{7}$$

The details of the construction of U are shown in Algorithm 1.

Algorithm 1 Computation of the Propagation List, U.

```
Let $\mathfrak{P}$ be the set of all the *tiles* and $\mathcal{B}^{\mathcal{P}}$ $(\forall \mathcal{P} \in \mathfrak{P})$ the quality measure, then
Set initially $V \leftarrow \mathfrak{P}$, $U \leftarrow [\emptyset]$ and $\mathcal{N}_U \leftarrow V$
**repeat**
    $\mathcal{P}^* \leftarrow \max_{\mathcal{P} \in \mathcal{N}_U} \mathcal{B}^{\mathcal{P}}$
    Concatenate $\mathcal{P}^*$ at least of the sequence: $U \leftarrow U + [\mathcal{P}^*]$
    Update $V \leftarrow V \backslash \{\mathcal{P}^*\}$
    Update $\mathcal{N}_U$ according to (7).
**until** $V = \emptyset$
```

We propose a phase propagation–based procedure for computing the *tile*'s sign and DC, and thus the PF phase Φ. Such a procedure starts at a seed *tile*. Our strategy consists of growing a partial solution by including the neighbor *tile*–phase with the best quality measure. The phase growing is determined by the propagation map, U, (computed with Algorithm 1) and requires of computing the sign, $\sigma^{\mathcal{P}_b}$, and the corresponding DC, $\delta^{\mathcal{P}_b}$, of the *tile* to be attached, $\mathcal{P}_b$. The *tile* $\mathcal{P}_b$ is attached to a neighbor *tile* , denoted here by, $\mathcal{P}_a$, in the partial solution with the largest quality measure. Then the phase $\Phi^{\mathcal{P}_b}$ is estimated with

$$\Phi^{\mathcal{P}_b} = \sigma^{\mathcal{P}_b} \tilde{\phi}^{\mathcal{P}_b} + \delta^{\mathcal{P}_b}; \tag{8}$$

the coupling variables ($\sigma^{\mathcal{P}_b}$, $\delta^{\mathcal{P}_b}$) are computed with $\delta^{\mathcal{P}_b} = \delta^*_{i^*}$, and $\sigma^{\mathcal{P}_b} = (-1)^{i^*+1}$; where i^* and δ^*_i are the solutions to the optimization problems:

$$\delta^*_i \quad = \quad \arg\min_{\delta \in \mathfrak{R}} \tilde{F}_i(\delta) \tag{9}$$

and

$$i^* = \arg\min_{i \in \{1,2\}} \tilde{F}_i(\delta^*_i). \tag{10}$$

The cost functions $\tilde{F}_i$, for $i \in \{1, 2\}$, penalize the third derivatives of the phase (second derivatives of the frequency) in the coupling region for the respective cases in which the sign of the phase is correct or needs to be corrected. Thus, by minimizing $\tilde{F}_1$ with respect to (*w.r.t.*) δ we prefer couplings with smooth changes in the frequency, assuming a correct sign. On the other hand, $\tilde{F}_2$ takes into account a possible sign change. $\tilde{F}_i(\delta)$ can be understood as the discrete version of:

$$F_i(\delta) \;=\; \int_{r\in\mathcal{P}_a\cup\mathcal{P}_b} \left|\frac{\partial^3}{\partial t^3}[\sigma_i(r)S(r)+\delta(r)]\right|^2 dr; \tag{11}$$

with $t \in \{x, y\}$ defining the partial derivative direction: x for a horizontal coupling case and y for vertical case; S is the subimage defined by $\mathcal{P}_a \cup \mathcal{P}_b$ and δ is defined as

$$\delta(r) \;\overset{def}{=}\; \begin{cases} \delta, & \text{if } r \in \mathcal{P}_b, \\ 0, & \text{if } r \in \mathcal{P}_a. \end{cases} \tag{12}$$

and

$$\sigma_i(r) \;\overset{def}{=}\; \begin{cases} (-1)^{i+1}, & \text{if } r \in \mathcal{P}_b, \\ 1, & \text{if } r \in \mathcal{P}_a. \end{cases} \tag{13}$$

We obtain the discrete version of $F_1(\delta)$ and $F_2(\delta)$ by approximating the partial derivatives with finite differences, see subsection 3.B. In such a case, the support of the integral (summation) is confined to a coupling region Ω of 6 columns and m rows (for *tiles* of $m \times m$ pixel size), this is illustrated in Fig. 4. In the case of a vertical coupling Ω has m columns and 6 rows. It is important to remark that the solutions δ_1^* and δ_2^* of the optimization problems [*i.e.* the discrete versions of (11)] can be efficiently computed with simple closed formulas, see next subsection.

3.B. Implementation Details

The cost functions $F_1(\delta)$ and $F_2(\delta)$ [eq. (11)] are approximated by means of finite differences. Then the integral (summation) support is confined to a coupling region Ω. If the *tiles* A and B are east (horizontally) coupled, then Ω is the pixels set in the subimage s of 6 columns and m rows (for *tiles* of $m \times m$ pixel size). In this subsection we present the formulas for the east coupling illustrated in Fig. 4. They are straightforward generalized to the other 3 coupling cases: north, south and west. In the case of a north and south (vertical) coupling, the region Ω has m columns and 6 rows.

In the east coupling case, the *tile*-wise constant term (DC) and the sign are computed by minimizing the following discrete cost functions:

$$\begin{aligned}\tilde{F}_1(\delta) \;=\; \sum_{i=0}^{m-1} \Big\{ & \{s[i][0] - 3s[i][1] + 3s[i][2] - (s[i][3] + \delta)\}^2 + \\ & \{s[i][1] - 3s[i][2] + 3(s[i][3] + \delta) - (s[i][4] + \delta)\}^2 + \\ & \{s[i][2] - 3(s[i][3] + \delta) + 3(s[i][4] + \delta) - (s[i][5] + \delta)\}^2 \Big\},\end{aligned} \tag{14}$$

and

$$\begin{aligned}\tilde{F}_2(\delta) \;=\; \sum_{i=0}^{m-1} \Big\{ & \{s[i][0] - 3s[i][1] + 3s[i][2] + (s[i][3] - \delta)\}^2 + \\ & \{s[i][1] - 3s[i][2] - 3(s[i][3] - \delta) + (s[i][4] - \delta)\}^2 + \\ & \{s[i][2] + 3(s[i][3] - \delta) - 3(s[i][4] - \delta) + (s[i][5] - \delta)\}^2 \Big\}.\end{aligned} \tag{15}$$

The cost function $\tilde{F}_1$ and $\tilde{F}_2$ are the discrete versions of F_1 and F_2 [Eq. (11)], respectively. The optimum δ–values, for $\tilde{F}_1$ and $\tilde{F}_2$ (respectively), can be computed with the closed formulas:

$$\delta_1^* = \frac{\sum_{i=0}^{m-1} \sum_{j=0}^{5} (-1)^j \begin{pmatrix} 5 \\ j \end{pmatrix} s[i][j]}{6m}, \tag{16}$$

$$\delta_2^* = \frac{\sum_{i=0}^{m-1} \sum_{j=0}^{5} (-1)^{j+\delta_b} \begin{pmatrix} 5 \\ j \end{pmatrix} s[i][j]}{6m}; \tag{17}$$

where

$$\delta_b \overset{def}{=} \begin{cases} 1, & \text{if } j > 2, \\ 0, & \text{otherwise.} \end{cases} \tag{18}$$

4. Multigrid phase refinement

The propagated phase, computed with the procedure presented in last section, is good enough for many practical uses. However, by noise effect some artifacts could be introduced. For improving the phase quality, we propose a refinement postprocess that removes noise and eliminates possible artifacts produced by the coupling process. Such a refinement process is based on the one proposed by Rivera in Ref. [8]. That refinement has demonstrated a better behavior than a simple homogeneous filtering of the phase [17]. In this work, we implement a multigrid version of the refinement algorithm. Multigrid methods are a particular case of domain decomposition methods used for accelerating convergence of iterative algorithm for solving systems of partial differential equation (PDEs) [28]. Such PDEs are generally obtained as the Euler-Lagrange equations in a variational framework or, as in our case, from their discrete version. Multigrid methods has successfully been used for implementing phase unwrapping, robust quadrature filters and phase filtering procedures [29–31].

Following Ref. [8], we assume that the coupled phase, Φ, is a close approximation of the real phase, f, the magnitude of the quadrature filter, $\hat{b}$, approximates well the FP magnitude and an estimation of the background $\hat{a}$ is available. Then the task is to compute a residual phase (correction field), ψ, such that $f_r = \Phi_r + \psi_r$. If $|\psi_r| \ll |\Phi_r|$ then the Taylor's first order approximation can be used and, from model (1), one can define the residual:

$$E\left(\psi, r\right) \; = \; I(r) - \hat{a}(r) - \hat{b}(r)[\cos\Phi(r) - \psi(r)\sin\Phi(r)] \approx 0. \qquad (19)$$

The approximation of a non-linear residual by first order Taylor's series has shown to be effective in the solution of many problems of image processing and computer vision, for instance optical flow computation, see [32] and references therein. This approximation has also been used in closed fringe analysis [7, 8] and phase stepping algorithms [17]. Then, according to Ref. [8] the potential to minimize is given by

$$\begin{aligned} U(\psi, \omega) \; = \; & \sum_{r \in R} [\omega_r^2 E^2(\psi, r) + \mu(1-\omega_r)^2 + \gamma\psi^2(r)] + \\ & \lambda \sum_{<q,r,s> \in R} [\Phi(q) + \psi(q) - 2(\Phi(r) + \psi(r)) + \Phi(s) + \psi(s)]^2; \end{aligned} \qquad (20)$$

where the weights $\omega_r \in [0,1]$ can be understood as outlier detectors, μ and λ are parameters that control the outlier detection and the smoothing processes, respectively. The outlier detection mechanism will drop out the data (by weighting them with $\omega \approx 0$) and the regularization term will interpolate a smooth solution, that allows to remove large residuals (product of artifacts). Next, if the interpolated phase produces a small residual, then in following iterations the data term will be considered in the computation, see experiments in Section 5. The term $\psi^2(r)$, weighted by γ, was proposed in Ref [17] for stabilizing the refinement process, and promotes small correction fields. In this work (as in Ref [17]) we set $\gamma = 1$.

We understand the refinement process as the application of an operator to the coarse phase Φ, such an operator $\mathcal{R}$ is defined as:

$$\mathcal{R}_{\mu,\lambda,I}\Phi \overset{def}{=} \Phi + \psi^*; \tag{21}$$

where $\{\psi^*, \omega^*\} = \arg\min_{\psi,\omega} U(\psi,\omega)$. According to Ref. [8], the refinement operator is applied iteratively, $\Phi_{n+1} = \mathcal{R}_{\mu,\lambda,I}\Phi_n$, until $|\psi_n^*| \approx 0$.

Multigrid methods require of defining two more operators: a contraction operator, $\mathcal{D}_2$, and an expansion operator, $\mathcal{E}_2$ [28]. The $\mathcal{D}_2$ operator combines a downsampling process (by a factor of 2) and a smoothing process (implemented as a simple homogeneous diffusion [33,34]). The expansion operator, $\mathcal{E}_2$, combines an upsampling (by a factor of 2) and an interpolation of the upsampled pixels. In this work a bilinear interpolation is used.

The multigrid refinement process is following explained. We assume that the propagated phase, Φ_0, (computed with the algorithm proposed in section 3) needs to be refined, then the first step consists of computing a contracted coarse phase,

$$\Phi_1 = \mathcal{D}_2\Phi_0. \tag{22}$$

Then, such a contracted phase is refined and expanded to the original size,

$$\tilde{\Phi}_0 = \mathcal{E}_2\mathcal{R}_{\mu,\lambda/4,\mathcal{D}_2 I}\Phi_1. \tag{23}$$

Afterwards, such an up-refined phase $\tilde{\Phi}_0$ is used as initial condition for computing the final refined phase, Φ_0^*, at the original dimension:

$$\Phi_0^* = \mathcal{R}_{\mu,\lambda,I}\tilde{\Phi}_0. \tag{24}$$

Last two level refinement process [Eqs. (22), (23) and (24)] can be generalized to multiple levels in a multigrid pyramidal fashion, i.e. for refining the contracted phase in (23), one can use as initial condition the phase Φ_1^* that results of a similar refinement process at an upper level. That leads us to define the refinement process as a recursive procedure which top level is determined by the highest frequency in the FP. This refinement procedure is represented in Fig. 5. The first column shows the unwrapped final refined phase at each label. The top level refined phase is expanded (upsampled and interpolated) and used as initial (coarse) phase for the refined in the lower level. For illustration purposes, second and third columns show the rewrapped phase and the reconstructed FP, respectively. The procedure details are shown in algorithm 2.

Algorithm 2 Multigrid Phase Refinement (MPR)

Let I the interferogram, Φ a coarse phase, $k > 0$ the number of levels and (μ, λ) the algorithm parameters, then MPR procedure is given by

```
procedure REFINE($\Phi, I, \lambda, \mu, k$)
    if $k > 1$ then
        $\hat{\Phi} \leftarrow$ REFINE $(\mathcal{D}_2\Phi, \mathcal{D}_2 I, \lambda/4, \mu, k-1)$        ▷ Refinement at an upper level
        $\Phi \leftarrow \mathcal{E}_2\hat{\Phi}$
    end if
    $\Phi \leftarrow \mathcal{R}_{\mu,\lambda,I}\Phi$
    return $\Phi$
end procedure
```

5. Experiments

In this section we demonstrate the method performance by numerical experiments. The refinement algorithm parameters were fixed for the whole set of experiments. The multigrid pyramid level number was $k = 3$, including the original level and the parameters were set as the recommended in Ref. [8]: $\mu = 0.01$ and $\lambda = 0.2$ (with $\gamma = 1$).

Fig 6 shows a set of fringe patterns (first column) and the respective results computed with our algorithm. Second column shows the computed phases that result of the phase propagation stage (proposed in section 3) and the third column shows the final phase refined with the method in section 4. The results demonstrate that the proposed method (*tile*–based propagation and refinement) is robust to: noise, variations in the FP contrast and high variations in the fringes frequency bandwidth. In many cases the propagated phase is of good enough quality for practical uses. However, wide quadrature filters are prone to wrongly estimate the phase at noisy pixels with high frequencies. Hence the proposed propagation procedure could correctly recover the phase at the surrounding area of corrupted *tile* phases and the multigrid refinement can restore the phase at such problematic sites. This performance can be noted in the computed propagated and refined phases in rows 1 and 3 of Fig. 6.

Table 1 presents the resume of the computational times corresponding to phases in Fig. 6. The code was implemented in C and executed in a Pentium IV 2.8 MHz with 1GByte in RAM. No extra care was taken for implementing a computationally efficient code. The computational performance of our algorithm is favorably better than the performance of the regularized phase tracker: non-linear with fringe pattern contrast information (bRPT) and linearized (LRPT) versions. The evaluated bRPT and LRPT correspond to the cost functions (4) and (13) in Ref. [7], respectively. In particular the modulation component, $\hat{b}$, for the bRPT algorithms was estimated in a preprocessing stage using the method in Ref. [35]. This preprocessing time is not considered in Table 2. The computational times of the bRPT and LRPT for the FP in Fig. 6 are shown in Table 2 (compare with the propagation times of our framework in 4th column in Table 1). Our algorithm is faster than the LRPT and the results are of the quality as those computed with the bRPT algorithm. Fig. 7 shows the rewrapped computed phase of the FP in the 6th row of Fig. 6 computed with the LRPT and bRPT.

Next experiments have the purpose of demonstrating the capabilities of the multigrid refinement process. In particular, the sensibility to the *tile* size and to large errors in the initial coarse phase. The results in Fig. 8 correspond to the FP in the third row in Fig. 6, in this case the experiments were done by changing the *tile* size. One can observe that if the *tile* size is chosen too large (e.g. 32×32 pixels) then the resulted phase may be corrupted by artifacts product of closed fringes in *tile* regions and therefore the local orientation is wrongly computed, see panel 8a. Such a problems is corrected by selecting a smaller *tile* size: panels 8b–d. However, while the *tile* size is reduced, the computational time of the propagation stage is increased. So that in all the experiment shown in this work we have used a *tile* size equal to 16×16 pixels that represents a compromise between the results quality and the computational time.

The last experiment shown in Fig 9 demonstrates the robustness of the refinement process with respect to large deformations in the coarse initial phase. In this experiment the coarse initial phase appear in the first row (central column) of Fig. 6 shown wrapped for illustration purposes. The Fig 9 shows two sequences (top down): first column shows the weight–map evolution and the second column shows the refine phase. In the initial iterations the weights show that the Taylor's series linearized model produces large residuals. Therefore, small–valued weights (shown in dark) reduce the contribution to the total cost (20) of large residuals. Note that the adaptive algorithm reduces systematically the error phase with the iterations. Such a behavior is observed in the weight-map that finally detects small residuals. Such a capability of the algorithm for reduction large residual is agree with the experimental evidence shown in Refs. [7, 8, 17]. We remark that, for illustration purpose, this particular experiment was done using only the lower level of the pyramidal data; the computational convergence can be accelerated if the multigrid approach had been used.

6. Conclusions

We have presented a new framework for fast phase recovering from a single fringe pattern with closed fringes. Our proposal takes advantage of fast algorithms widely used in last decades for open fringe patterns. In particular, we implemented simple quadrature Gabor's filters in the frequency domain by means of the Fast Fourier Transform (FFT). We noted that the computed phases with two, horizontal and vertical, oriented wide bandwidth filters can be used as prime material for recovering the phase from patterns with closed fringe. Alternatively, the local phase can be computed by weighting the responses of a quadrature filter bank (Gabor's Filters [23], Monogenic Filters [9, 24], Riesz's transform [2–4], etc. In any case, the local sign need to be corrected for having a global solution. In this paper we have proposed a general framework for efficiently computing the local sign and computing the correct global phase.

We presented a novel criterion (based on a local orientation quality measure) for choosing between the phases computed using horizontally and vertically oriented quadrature filters. Our criterion uses the Knutsson's structure tensor for estimating the fringe orientation and for defining the propagation sequence. Moreover, for becoming robust the method to noise, we proposed to perform the propagation of the phase in a new image element named *tile*. Once an unwrapped *tile*–phase is estimated, the fringe analysis problem consists on estimating the *tile*–phase sign, $\sigma^{\mathcal{P}}$, and an additive constant term, $\delta^{\mathcal{P}}$. The final phase quality is improved by applying a fast multigrid refinement process presented in this work. Our method has demonstrated to be computationally efficient in both, real and synthetic data. Moreover, additional computational advantage could be obtained if the inverse Fourier transforms (required for computing the the quadrature filters responses) and the *tile*–based unwrapping were implemented in parallel.

List of Figures

List of Tables

Acknowledges

This research was supported in part by CONACYT (Grants 46270 and 61367) and CONCYTEG (Grant 06-02-K117-95-A02), Mexico. O. Dalmau also acknowledges a scholarship from the CONACYT research grants 40721-Y (S. Botello) and 46270 (J. L. Marroquin).

References

1. J. Marroquin, R. Rodriguez-Vera, and M. Servin, “Local phase from local orientation by solution of a sequence of linear systems,” J. Opt. Soc. Am. A , vol. 15, no. 6, pp. 1536–1544, 1998.
2. K. G. Larkin, D. Bone, and M. A. Oldfield, “Natural demodulation of two-dimensional fringe patterns: I. General background to the spiral phase quadrature transform,” J. Opt. Soc. Am. A , vol. 18, pp. 1862–1870, 2001.
3. K. G. Larkin, “Natural demodulation of two-dimensional fringe patterns: II. Stationary phase analysis of the spiral phase quadrature transform,” J. Opt. Soc. Am. A , vol. 18, pp. 1871-1881, 2001.
4. K. G. Larkin, “Uniform estimation of orientation using local and nonlocal 2-D energy operator,” Opt. Express , vol. 13, pp. 8097–8121, 2005.
5. M. Servin, J. Marroquin, and F. Cuevas, “Demodulation of a single interferogram by use of a two-dimesional regularized phase-tracking technique,” Appl. Opt. , vol. 36, pp. 4540–4548, 1997.
6. M. Servin, J. Marroquin, and J. A. Quiroga, “Regularized quadrature and phase tracking from a single closed-fringe interferogram,” J. Opt. Soc. Am. A , vol. 21, pp. 411–419, 2004.
7. R. Legarda-Sáenz and M. Rivera, “Fast half-quadratic regularized phase tracking for non normalized fringe patterns,” J. Opt. Soc. Am. A , vol. 23, no. 11, pp. 2724–2731, 2006.
8. M. Rivera, “Robust phase demodulation of interferograms with open and closed fringes,” J. Opt. Soc. Am. A , vol. 22, pp. 1170–1175, 2005.
9. J. A. Guerrero, J. L. Marroquin, M. Rivera and J. A. Quiroga, “Adaptive monogenic filtering and normalization of ESPI fringe patterns,” Opt. Lett. , vol. 30, pp. 3018-3020, 2005.
10. J. C. Estrada, M. Servin and J. L. Marroquin, “Local adaptable quadrature filters to demodulate single fringe patterns with closed fringes,” Opt. Express , 15, 2288–2298, 2007.
11. J. L. Marroquin, M. Servin, and R. Rodriguez-Vera, “Adaptive quadrature filters and the recovery of phase from fringe pattern images,” J. Opt. Soc. Am. A , vol. 14, 1742–1753 (1997).
12. Q. Kemao and H Soon, “Sequential demodulation of a single fringe pattern guided by local frequencies,” Opt. Lett. , 32, 127–129, 2007.

13. W. W. Macy, “Two-dimensional fringe-pattern analysis,” Appl. Opt. , vol. 22, pp. 3898-3901, 1983.

14. T. Kreis, “Digital holographic interference-phase measurement using the Fourier transform method,” J. Opt. Soc. Am. A , vol. 3, pp. 847–855, 1986.

15. T. R. Judge, C. Quan, and P. J. Bryanston Cross, “Holographic deformation measurements by Fourier transform technique with automatic phase unwrapping” *Opt. Eng.*. vol. 31, pp. 533–43, 1992.

16. H. Knutsson, “A tensor representation of 3-D structure,” in *5th IEEE-ASSP and EURASIP Workshop on Multidimensional Signal Processing*, Noordwijkerhout, The Netherlands, September 1987.

17. M. Rivera, R. Bizuet, A. Martínez, and J. A. Rayas, “Half-quadratic cost for computing arbitrary phase shifts and phase: Adaptive out of step phase shifting,” Opt. Express , vol. 14, pp. 3204–3213, 2006.

18. X. Yang, Q. Yu and S. Fu. ”An algorithm for estimating both fringe orientation and fringe density,” Opt. Commun. , 274, 286–292, 2007.

19. H. Knutsson, “Representing local structure using tensors,” in *In The 6th Scandinavian Conference in Image Analysis*, Oulu, Finland, June 1989, pp. 244–251.

20. H. Knutsson and M. Andersson, “Implications of invariance and uncertainty for local structure analysis filter sets”, *Signal Processing: Image Communications*, vol. 20, pp. 569–581, 2000.

21. B. Jähne, *Digital Image Processing; Concepts, Algorithms, and Scientific Applications*, 2nd ed. Berlin: Springer-Verlag, 1991.

22. L. Haglund, H. Knutsson, and G. H. Granlund, “Scale and orientation adaptive filtering,” in *Proceedings of the 8th Scandinavian Conference on Image Analysis*. Tromsö, Norway: NOBIM, May 1993, report LiTH–ISY–I–1527, Linköping University.

23. I. W. Bowler and K. Paler, “A Gabor filter approach to fringe analysis,” *In Proc. Int. Conf. Pattern Recog. (ICPR’86)*, 558–560, 1986.

24. M. Felsberg and G. Sommer, “The monogenic signal,” IEEE Trans. on Signal Process., 49(12), 3136–3144, 2001.

25. K. H. Womak, “Interferometric phase measurement using spatial synchronous detection,” Opt. Eng., vol. 23, pp. 391–395, 1984.

26. M. Takeda, H. Ina, and S. Kobayashi, “Fourier-transform method of fringe-pattern analysis for computer-based topography and interferometry,” J. Opt. Soc. Am. , vol. 72, pp. 156–160, January 1982.

27. M. Rivera and J. L. Marroquin, “Half-quadratic cost functions for phase unwrapping,” Opt. Lett. , vol. 29, pp. 504-506, 2004.

28. W. L. Briggs, V. E. Henson and S. F. McCormick, *A Multigrid Tutorial*, 2nd Edition, SIAM publications, Philadelphia, 2000.

29. M. D. Pritt, ”Multigrid phase unwrapping for interferometric SAR,” in *Proceedings of IGARSS*, vol. 1,pp. 562–564, 1995.
30. S. Botello, J. L. Marroquin and M. Rivera, “Multigrid algorithms for processing fringe pattern images,” Appl. Opt., vol. 37, pp. 7587–7595, 1998.
31. G. Dardyk and I. Yavneh, “A multigrid approach to two-dimensional phase unwrapping,” Numerical Linear Algebra with Applications, vol. 11, pp. 241–259, 2004.
32. D. J. Fleet and Y. Weiss, “Optical flow estimation,” in Mathematical models for Computer Vision: The Handbook. N. Paragios, Y. Chen, and O. Faugeras (eds.), Springer, 2005.
33. A. P. Witkin, “Scale-space filtering,” Proc. 8th Int. Joint Conf. Art. Intell., Karlsruhe, Germany, 10191022, 1983.
34. J. J. Koenderink, “The structure of images,” Biol. Cyber., vol. 50, pp. 363–370, 1984.
35. J. A. Quiroga and M. Servin, “Isotropic n-dimensional fringe pattern normalization,” Opt. Commun. , vol. 224, pp. 221-227, 2003.

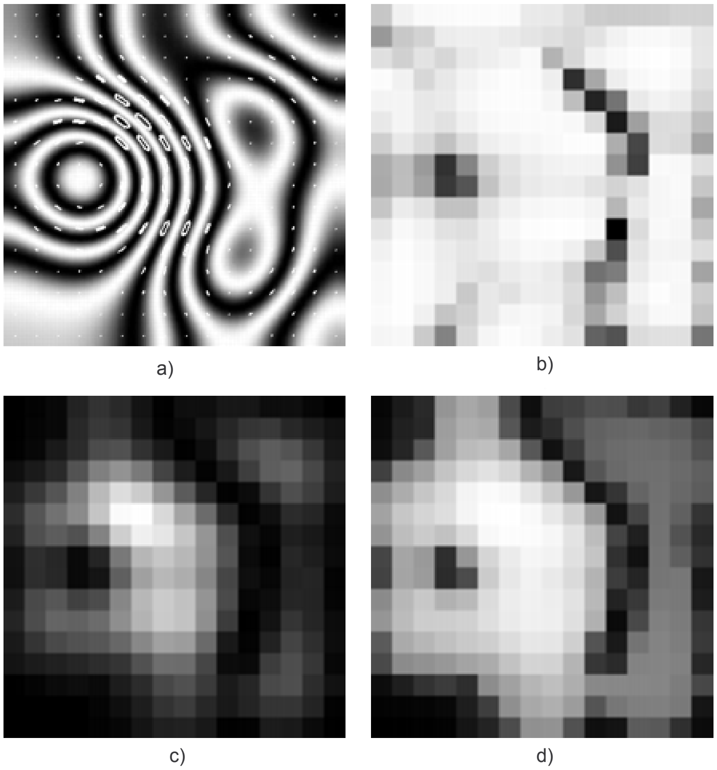

Fig. 1. a) Level set of the tensors' quadratic form overset on the FP, I, of Fig. 2b, see text. b) Coherency map, $\mathcal{C}$. c) Quality measure map, $\mathcal{B}$. d) Propagation map, U.

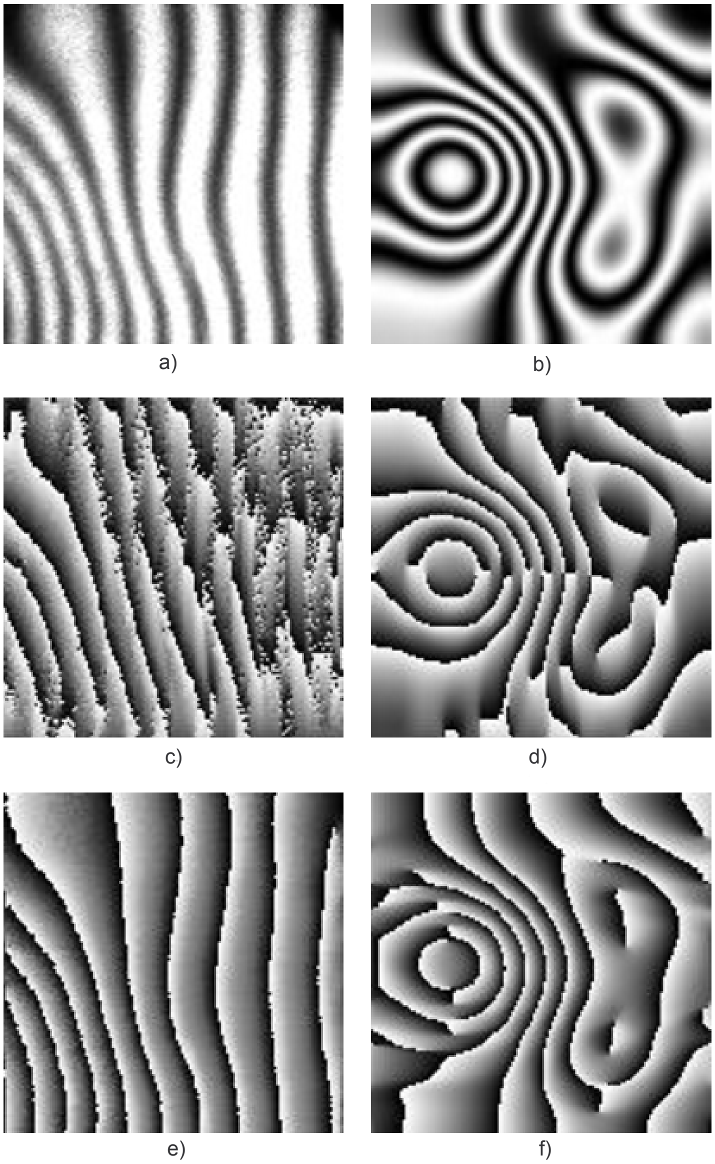

Fig. 2. a) Fringe Pattern (FP) with open fringes, b) FP with closed fringes, c) and d) Phases computed with a horizontally oriented quadrature filter, ϕ_v. e) and f) Phases computed with a vertically oriented quadrature filter, ϕ_u.

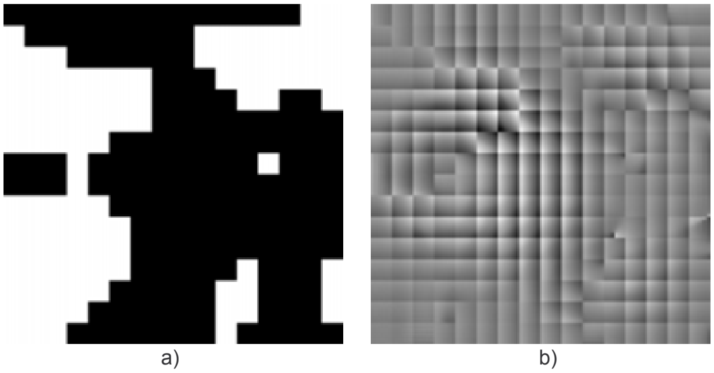

Fig. 3. a) Selection map: in white if the phase is taken from ϕ_v and in black if the phase is taken from ϕ_u. b) Unwrapped phase by *tiles*, $\tilde{\phi}$.

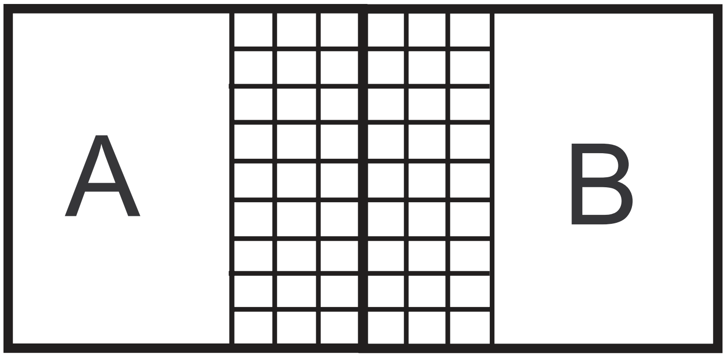

Fig. 4. Illustration of the *tiles* coupling band.

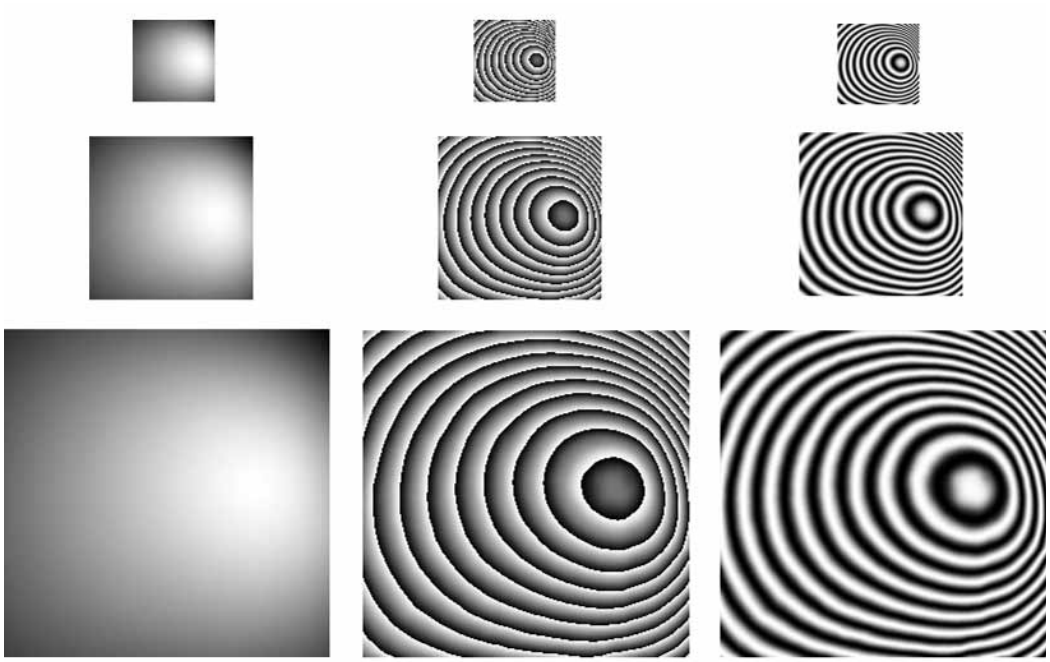

Fig. 5. Illustration of the multigrid refinement process.

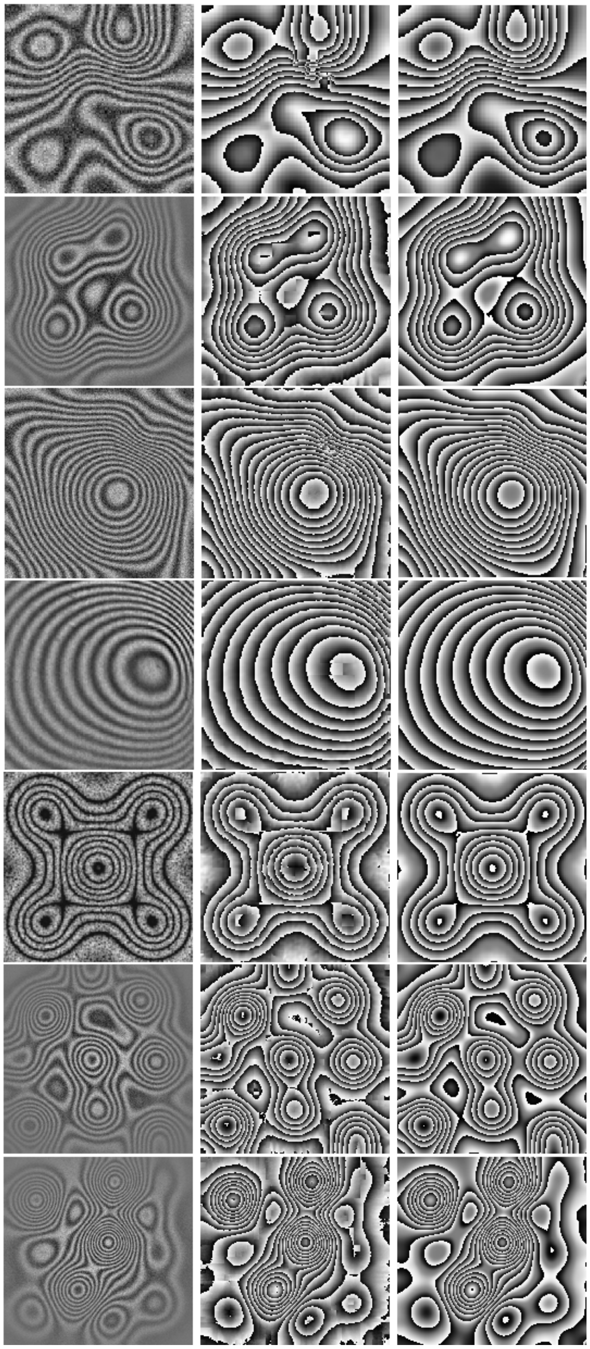

Fig. 6. Recovered phase from single closed fringe patterns with the proposed method. Fringe pattern, I (first column). Resultant estimated phase of the propagation stage, Φ (middle column). Refined phase, Φ^*, that results of the complete proposed procedure (last column).

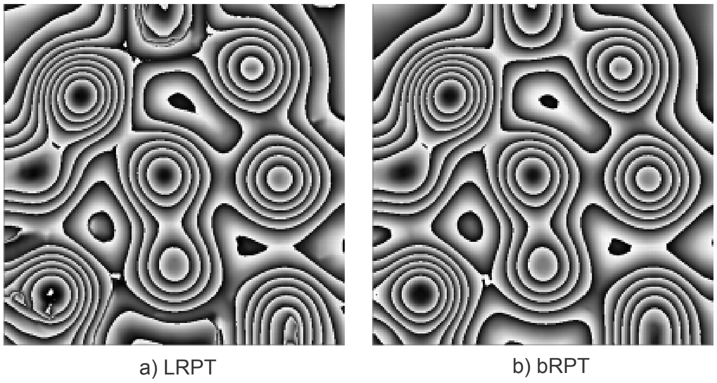

a) LRPT

b) bRPT

Fig. 7. Computed phases (rewrapped for illustration purposes) with RPT algortihms from the FP in Fig. 6 (row 6). The phases correspond to the propagation step results.

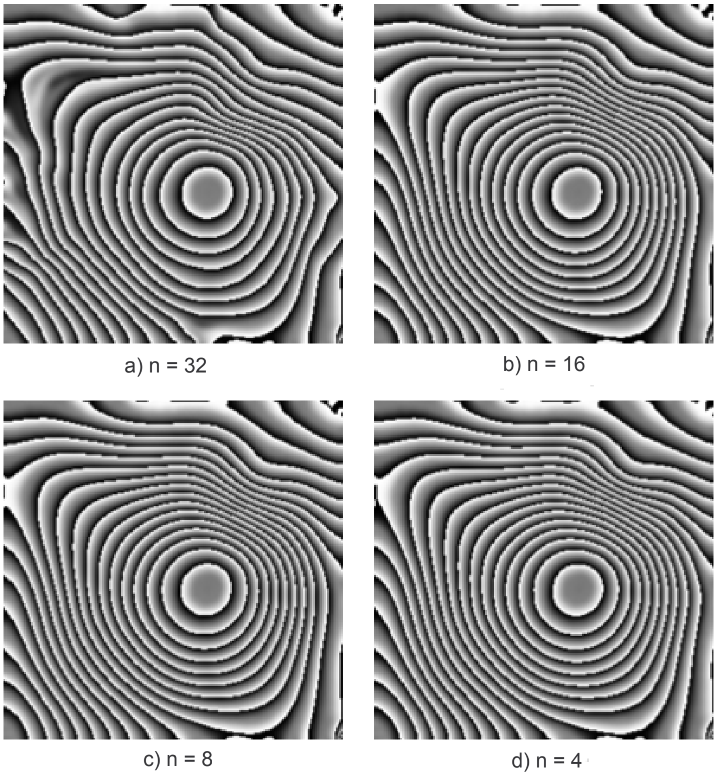

Fig. 8. Phase results computed by partitioning the the fringe pattern in *tiles* with size of $n \times n$ pixels.

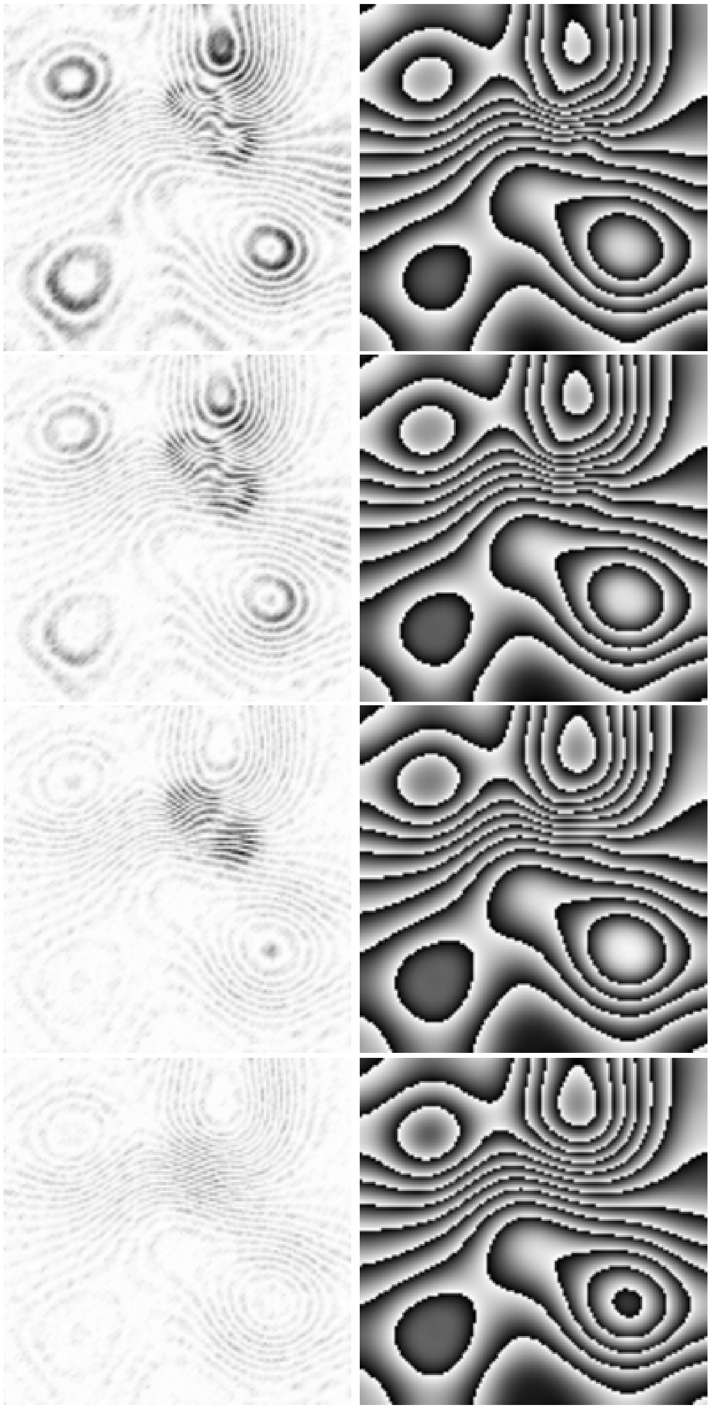

Fig. 9. Top-down: Refinement evolution of the weights and the phase, the phase is wrapped for illustration purposes in the refinement iterations (see text).

Table 1. Algorithm performance on real and synthetic fringe patterns.

Fringe pattern	Size	Quadrature	Propagation	Refinement	Total
Row in Fig. 6	in pixels	Filters (secs.)	time (secs.)	time (secs.)	time (secs.)
1	128×128	0.040	0.194	0.234	0.468
2	256×256	0.170	0.893	0.906	1.969
3	256×256	0.170	0.877	0.922	1.969
4	256×256	0.170	0.861	0.890	1.921
5	256×256	0.170	0.892	0.906	1.968
6	512×512	1.090	4.223	3.797	9.110
7	512×512	1.090	4.254	3.797	9.141

Table 2. Propagation time for RPT algorithms, versions: linealized (LRPT) and non–linear (bRPT).

Fringe pattern	LRPT	bRPT
Row in Fig. 6	(secs.)	(secs.)
1	2.45	4.11
2	3.85	15.96
3	6.79	28.57
4	5.83	27.02
5	8.97	27.16
6	17.98	108.32
7	24.11	107.63